ELSEVIER

Chemical Engineering Journal 138 (2008) 498–509

Chemical Engineering Journal

www.elsevier.com/locate/cej

CFD modelling of $BaSO_4$ precipitation inside microemulsion droplets in a semi-batch reactor

Alper A. Öncül [a,*], Björn Niemann [b], Kai Sundmacher [b,c], Dominique Thévenin [a]

[a] *Institut für Strömungstechnik und Thermodynamik, Lehrstuhl für Strömungsmechanik und Strömungstechnik (ISUT/LSS), Otto-von-Guericke-Universität-Magdeburg, Universitätsplatz 2, D-39106 Magdeburg, Germany*

[b] *Max-Planck-Institut für Dynamik komplexer technischer Systeme, Sandtorstrasse 1, D-39106 Magdeburg, Germany*

[c] *Institut für Verfahrenstechnik, Lehrstuhl für Systemverfahrenstechnik (IVT/SVT), Otto-von-Guericke-Universität-Magdeburg, Universitätsplatz 2, D-39106 Magdeburg, Germany*

Received 13 February 2007; received in revised form 5 July 2007; accepted 6 July 2007

Abstract

Nanoparticle production using microemulsion droplets has become a very interesting technique in the recent years. It allows a controlled adjustment of the particle size, which is an essential task due to the highly size-dependent properties of nanoparticles. For numerical investigations of this configuration a population balance model (PBM) framework based on discrete coordinates has been derived. An appropriate reduction concept is applied to obtain an efficient numerical solution. Although the resulting zero-dimensional (spatially homogeneous) calculations show a qualitatively good agreement with the experimental data for stoichiometric conditions, larger deviations have been observed for cases with a high concentration excess of one reactant inside the microemulsion droplets. Such deviations might result from the fact that the precipitation rate strongly depends on the local supersaturation. High concentration differences, especially near the feed lead to large local variations of the supersaturation profile. Thus, computational fluid dynamics (CFD) simulations have been performed for a refined analysis. This has been managed by implementing the reduced PBM model in the commercial CFD code FLUENT® 6.2 via user-defined scalars and functions. By this way, it becomes possible to investigate the reaction process for various three-dimensional inhomogeneous hydrodynamic conditions with acceptable computational times. The obtained results are finally compared with the homogeneous calculation results and with the experiments. Moreover, local variations within the reactor are also examined.

Keywords: CFD; Population balance model; Microemulsion; Precipitation; Barium sulfate; Nanoparticles

1. Introduction

The production of nanoparticles with well-defined properties of the resulting particle size distribution (PSD) is a challenging task for current research. An exact size control is an important issue due to the strong size dependence of chemical and physical nanoparticle properties resulting from quantum effects [1]. A strong influence on, e.g. melting point, fluorescence spectrum or chemical activity has been observed for a variety of materials when the particle size is below 100 nm. A promising and on laboratory scale well-established wet chemistry process, which allows an accurate size control during the production, is the precipitation of nanoparticles inside the water droplets of a microemulsion. Many different materials like semiconductors, metals, metal oxides, borides, carbonates and sulfates have already been successfully produced by this method (see overview by Niemann et al. [2]). An example for the quality of the produced nanoparticles is given in Fig. 1a. The shown $BaSO_4$ particles have a very narrow size distribution with a mean particle diameter of approximately 6.5 nm. Adityawarman et al. [3] showed in their experimental study that the mean particle diameter can be precisely adjusted between 6 and 35 nm by this technique.

The main reason for this excellent suitability of the microemulsion technique for the production of tailored nanoparticles is the adjustment of well-defined conditions for nucleation and growth by the limited amount of reactants inside the nano-sized droplets. The primarily formed nuclei, which consist only of a few molecules, are protected by the surrounding surfactant monolayer against uncontrolled growth and agglomeration.

* Corresponding author. Tel.: +49 391 6718195; fax: +49 391 6712840.
E-mail address: alper.oencuel@vst.uni-magdeburg.de (A.A. Öncül).

1385-8947/$ – see front matter © 2007 Elsevier B.V. All rights reserved.
doi:10.1016/j.cej.2007.07.073

Nomenclature

c_A	concentration of reactant A (mol/l)
c_B	concentration of reactant B (mol/l)
c_{feed}	reactant concentration in the feed (mol/l)
$c_{reactor}$	reactant concentration inside the reactor (mol/l)
d_D	droplet diameter (nm)
d_{imp}	impeller diameter (cm)
$\bar{d}_P$	mean particle diameter (nm)
f	normalized droplet number distribution
f_{ref}	reference droplet number distribution
k_B	Boltzmann constant (J/K)
k_L	solubility product (mol^2/l^2)
k_V	volume shape factor
k_{gro}^{eff}	effective growth rate constant (nm/s)
k_{nuc}^{eff}	effective nucleation rate constant ((m^3 s)$^{-1}$)
M_M	molecule allocation matrix for nucleation
M_P	molecular mass of the solid particle (g/mol)
N_A	number of dissolved Ba^{2+} ions (A) in one droplet
$N_{Avogadro}$	Avogadro's number (mol^{-1})
N_B	number of dissolved SO_4^{2-} ions (B) in one droplet
N_{crit}	critical number of molecules needed to form a stable nucleus
N_{feed}	total number of droplets fed per second (s^{-1})
$N_{l,max}$	maximum number of dissolved reactant molecules per droplet
N_M	total number of droplets in the reactor
$N_{M,0}$	initial total number of droplets in the reactor
N_P	number of $BaSO_4$ molecules per solid particle
$\bar{N}_P$	mean number of $BaSO_4$ molecules per solid particle
N_{rps}	impeller stirring rate (s^{-1})
N_s	total number of $BaSO_4$ molecules in solid state
N_0	total number of empty droplets
N_A^{total}	total number of dissolved Ba^{2+} ions (A) in the system
N_B^{total}	total number of dissolved SO_4^{2-} ions (B) in the system
P_A	one-dimensional Poisson distribution for dissolved Ba^{2+} ions (A)
P_B	one-dimensional Poisson distribution for dissolved SO_4^{2-} ions (B)
P_{2D}	two-dimensional probability density function distribution
P_{2D}^{eq}	two-dimensional equilibrium distribution of the reactants
Q_c	circulation capacity (m^3/s)
r_{gro}	growth rate (nm/s)
r_{nuc}	nucleation rate ((m^3 s)$^{-1}$)
Re	Reynolds number
S	supersaturation
t	time (s)
t_{feed}	feeding time (s)
T	temperature (K)
V_D	volume of one droplet (m^3)
V_{feed}	volume of the feed (ml)
$\dot{V}_{feed}$	feed rate (ml/min)
$V_{reactor}$	volume of the reactor (ml)
V_W	volume of the water phase in the reactor (m^3)

Greek symbols

α_{gro}	growth rate law exponent
α_{nuc}	nucleation rate law exponent
δ	Dirac-delta function
λ_A	mean droplet occupancy with Ba^{2+} ions (A)
$\lambda_{A,0,feed}$	initial mean droplet occupancy in the feed with Ba^{2+} ions (A)
λ_B	mean droplet occupancy with SO_4^{2-} ions (B)
$\lambda_{B,0}$	initial mean droplet occupancy in the reactor with SO_4^{2-} ions (B)
ρ_P	particle density (kg/m^3)
σ_{eff}	effective interfacial surface tension (J/m^2)
τ	time scale (s)
Ψ_T	growth rate coordinate transformation correlation (nm^{-1})

Thus, the formation of bigger particles by growth is completely governed by the droplet exchange, which provides new reactants in small amounts of a few molecules from other droplets. A schematic illustration of the particle formation mechanism for ionic reactants (salts) is given in Fig. 1b.

Process models for the microemulsion system are usually very complex due to the high number of distributed properties which result in multi-dimensional partial differential equations with integral terms. Solutions by discretization of deterministic population balance models and simulations of stochastic Monte-Carlo models have been presented in literature (see overview by Niemann et al. [2]). They show a good agreement between laboratory-scale experiments and simulations for the ideally mixed case. However, the computational demand is so high that it is practically impossible to take into account inhomogeneous hydrodynamic conditions. In order to analyse and improve the process on a technical scale, it is nevertheless important to consider real flow conditions, as obtained numerically by CFD. For such coupled studies reasonable model reductions have to be performed to decrease the computational effort. Therefore, a first reduced numerical model has been derived and implemented within an industrial CFD code in a previous work [4]. This tool has been used to investigate the stoichiometric reaction process for three-dimensional inhomogeneous hydrodynamic conditions with reasonable computation times.

Similar modelling studies for emulsions can be found in the literature. For instance, an emulsion polymerization process has been modelled for batch as well as semi-batch systems in [5,6]. Moreover, the application of a reduced model for an optimal control of population balances is presented in [7]. Vale and McKenna [8] investigated the coupling of the flow field simulation with

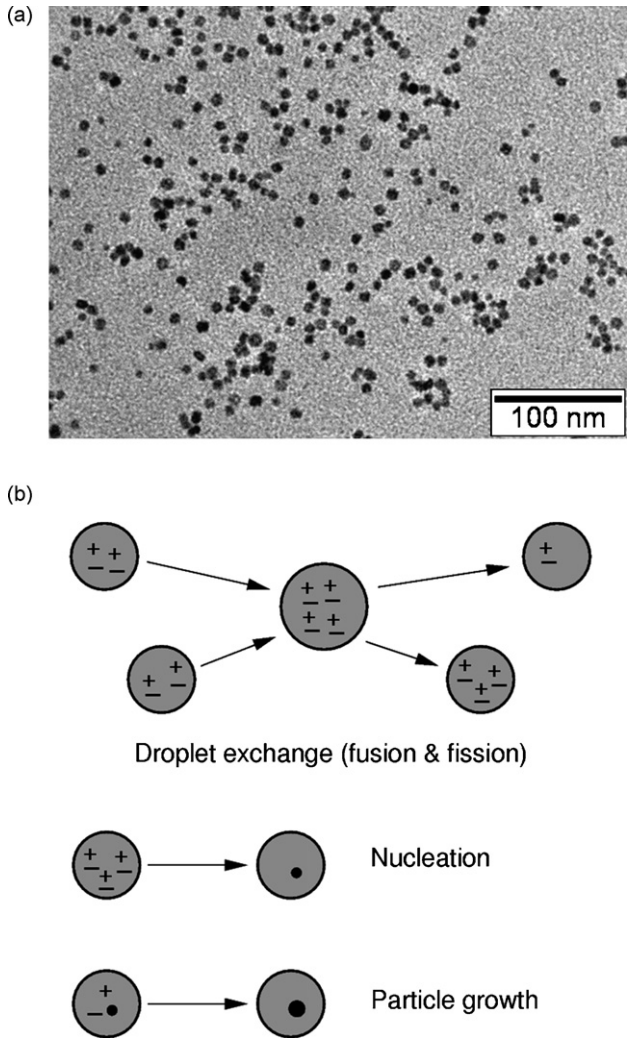

Fig. 1. (a) $BaSO_4$ nanoparticles produced by microemulsion precipitation (see details in the next section). (b) Important population dynamic mechanisms for the nanoparticle formation by precipitation of ionic reactants in microemulsion systems.

compartments method for the modelling of an emulsion polymerization in batch and continuous reactors. Recently, Singh and Kumar [9] modelled a microemulsion nanoparticle precipitation and validated their simplified model with the results of exact Monte-Carlo simulations.

2. Experimental setup

Experimental results by Adityawarman et al. [3] are used for the validation of the simulations. These authors investigated the nanoparticle precipitation of barium sulfate ($BaSO_4$) according to the following reaction scheme:

$$BaCl_2 + K_2SO_4 \rightarrow BaSO_4 \downarrow + 2KCl. \quad (1)$$

The two reactants $BaCl_2$ and K_2SO_4 were separately dissolved inside the water droplets of two identically composed microemulsions (continuous oil phase: cyclohexane, non-ionic technical surfactant: Marlipal O13/40). The droplets are almost monodisperse and their mean diameter is approximately 5 nm [3]. The precipitation experiments were performed in semi-batch operation mode in a Rushton-type stirred tank reactor with a 6-blade impeller rotating at 300 rpm in the clockwise direction ($Re = 4500$) and with 18 baffles [2,3]. The microemulsion containing the dissolved K_2SO_4 was filled inside the reactor and the second microemulsion with the dissolved $BaCl_2$ was added to the reactor with a constant feed rate. The influence of the initial concentrations of the two reactants inside the droplets on the final particle size distribution has been analyzed in detail. Therefore two sets of experiments have been performed. Within the first set the concentration of $BaCl_2$ in the feed was reduced stepwise from 0.1 to 0.01 mol/l while the concentration of K_2SO_4 was kept constant at 0.1 mol/l. In the second set the concentration of $BaCl_2$ in the feed was kept constant at 0.1 mol/l and the concentration of K_2SO_4 inside the reactor was reduced stepwise from 0.1 to 0.01 mol/l. The exact parameters of the five experiments investigated in this work are shown in Table 1.

Table 1
List of experiments used in this work

Case	K_2SO_4, $c_{reactor}$ (mol/l)	$BaCl_2$, c_{feed} (mol/l)
A	0.1	0.1
B1	0.1	0.05
B2	0.1	0.01
C1	0.05	0.1
C2	0.01	0.1

As a result of these experiments the influence of the initial concentration difference $\Delta c(t=0) = |c_{reactor} - c_{feed}|$ as a control parameter for the final particle size is identified. It could be shown that an increase of $\Delta c(t=0)$ leads to an increase of the final particle size. Detailed results are shown later on together with the comparison between experiments and simulations. A list of all important parameters used in the experiments is given in Table 2.

3. Numerical model

The dynamics of the nanoparticle precipitation inside microemulsion droplets are investigated according to three internal coordinates (distributed properties) and the three external coordinates (spatial position). The three internal coordinates are the numbers of barium and sulfate ions (N_A and N_B) as well as the number of $BaSO_4$ molecules per particle in solid state N_P. All coordinates are discrete and therefore a very accurate mass conservation is guaranteed. These three coordinates can be used to model the process if the following assumptions are made:

Table 2
Parameters of the experiments

Droplet diameter, d_D (nm)	5
Feed rate, $\dot{V}_{feed}$ (ml/min)	35
Feeding time, t_{feed} (s)	257.14
Temperature, T (K)	298.15
Volume of the microemulsion inside the reactor, $V_{reactor}$ (ml)	150
Volume of the microemulsion of the feed, V_{feed} (ml)	150

(a) Monodisperse water volume of each droplet.
(b) At maximum one particle per droplet.
(c) No agglomeration and breakage of particles.

These assumptions are justified in the present case: the droplet size distribution of droplets without particles is almost monodisperse [3]; only less than 1% of the droplets contain one particle; the nanoparticles observed on microscope pictures (see [3]) are no agglomerates or fragments of bigger particles. The first assumption is used as well for droplets with particles, since it is assumed that the water content remains constant during the expansion of droplets resulting from particle growth.

A direct solution of the fully coupled six-dimensional problem is practically impossible with current computational possibilities and solution methods. The computational demand for the solution of the three-dimensional PBM for the ideally mixed case without external coordinates is already extremely high. Therefore, a careful model reduction of the population balance model has to be performed before the external coordinates can be taken into account.

3.1. Population balance and reaction kinetics

3.1.1. Model reduction concept

The model reduction concept is based on reasonable assumptions concerning the distributed properties of the system, which allow the representation of the three-dimensional reference droplet number distribution $f_{\mathrm{ref}}(N_{\mathrm{A}}, N_{\mathrm{B}}, N_{\mathrm{P}}, t)$ by coupled balances with a lower dimension.

The first reduction step is obtained by a separation approach. The distribution of the two dissolved reactants and the particle size distribution can be split into two separated distributions if the redistribution of the reactants in the two daughter droplets is independent of the existence and size of a particle inside these droplets. The resulting distributions are a two-dimensional probability density function $P_{2\mathrm{D}}$ and a one-dimensional number density function f. Consequently, the reference number distribution f_{ref} can be calculated from

$$f_{\mathrm{ref}}(N_{\mathrm{A}}, N_{\mathrm{B}}, N_{\mathrm{P}}, t) \approx P_{2\mathrm{D}}(N_{\mathrm{A}}, N_{\mathrm{B}}, t) \cdot f(N_{\mathrm{P}}, t). \tag{2}$$

The computational demand needed for the solution of this coupled system is still too high for an implementation within a CFD code solving complex, three-dimensional unsteady flows [10–12] and a further reduction of the model has to be performed.

In a second reduction step a quasi-steady-state hypothesis is applied to the distribution of the dissolved reactants $P_{2\mathrm{D}}$. By this procedure $P_{2\mathrm{D}}$ is replaced by an analytically solvable equilibrium distribution $P_{2\mathrm{D}}^{\mathrm{eq}}$ and Eq. (2) is simplified to

$$f_{\mathrm{ref}}(N_{\mathrm{A}}, N_{\mathrm{B}}, N_{\mathrm{P}}, t) \approx P_{2\mathrm{D}}^{\mathrm{eq}}(N_{\mathrm{A}}, N_{\mathrm{B}}, t) \cdot f(N_{\mathrm{P}}, t) \tag{3}$$

with $P_{2\mathrm{D}}^{\mathrm{eq}}(N_{\mathrm{A}}, N_{\mathrm{B}}, t) = F(\lambda_{\mathrm{A}}(t), \lambda_{\mathrm{B}}(t))$, where λ_{A} and λ_{B} are obtained from Eqs. (6) and (7).

The application of an equilibrium distribution leads to the neglect of a slow-down effect resulting from the droplet exchange dynamics. If all reactants inside one droplet are depleted by nucleation and growth, further growth of this particle is only possible when a subsequent droplet exchange event provides new reactants from another droplet. The time period between depletion of reactants and a droplet exchange event is neglected in this model. Therefore this slow-down effect has to be considered by effective rate constants in the nucleation and growth rate approaches. These constants are determined by a parameter optimization [13] and they are slowed down by a factor of 10^{-3} to 10^{-7} compared to the corresponding rate constants obtained from bulk precipitation.

This second reduction step results in a significant decrease of the simulation times from hours to a few seconds depending on the processor speed and desired accuracy level [10,13]. Nevertheless, for the coupling with a CFD code the computational effort is still extremely high.

In the third and last reduction step the droplet number distribution f is replaced by two Dirac-delta functions. The first one represents all droplets without particle $N_0(t)$ and therefore it is located at $N_{\mathrm{P}} = 0$. The second Dirac-delta function stands for all droplets with particle $N_{\mathrm{M}}(t) - N_0(t)$ and it is located at the mean particle size represented by the mean number of molecules within one particle $\bar{N}_{\mathrm{P}}$. The approximation of f_{ref} is then given by

$$f_{\mathrm{ref}}(N_{\mathrm{A}}, N_{\mathrm{B}}, N_{\mathrm{P}}, t) \approx P_{2\mathrm{D}}^{\mathrm{eq}}(N_{\mathrm{A}}, N_{\mathrm{B}}, t) \cdot \begin{cases} N_0(t) \cdot \delta(N_{\mathrm{P}}, t) \\ \text{if } N_{\mathrm{P}} = 0 \\ (N_{\mathrm{M}}(t) - N_0(t)) \cdot \delta(N_{\mathrm{P}} - \bar{N}_{\mathrm{P}}, t) \\ \text{if } N_{\mathrm{P}} \geq N_{\mathrm{crit}} \end{cases} \tag{4}$$

The total number of droplets without particle $N_0(t)$ and the total number of droplets $N_{\mathrm{M}}(t)$ can be calculated by Eqs. (10) and (12) given in Section 3.1.3. Due to the loss of information concerning the PSD a small error has to be accepted in the solution of this model. The mean growth rate in Eq. (11) has to be calculated from the mass averaged mean particle size and not from a size average (see Eqs. (14) and (15)). The mass averaged particle size predicts in our case a higher mean particle size and therefore a higher growth rate. A significant effect on the final results of the presented simulations can be excluded due to the very narrow and mono-modal PSDs in this system which only lead to a small difference between the two mean values.

In conclusion the highest error in the presented model reduction concept is reduction step from Eq. (2) to Eq. (3). The neglect of the droplet exchange dynamics forces an alternative consideration of the droplet exchange by effective rate constants in the nucleation and growth rate approaches. Nevertheless, the qualitatively good fit obtained with this approach presented in [13] justifies the applicability of this reduction step.

3.1.2. Determination of P_{2D}^{eq}

The distribution of reactants inside the microemulsion droplets has been investigated first by Atik and Thomas [14]. They found out that a dissolved salt is distributed according to a Poisson distribution. In a more recent study by Hatton et al. [15] the interactions between the different dissolved ions were taken into account. They showed that the distribution of

the reactants strongly depends on the redistribution during the droplet exchange. Two limiting cases of the distribution can be identified: (i) the Poisson distribution for the case that repulsive and cooperative forces between the ions are almost the same and (ii) bimodal distributions with a lot of empty droplets in the case of strong cooperative forces between the different ions. The presented model approach allows the implementation of any arbitrary probability density distribution. Studies according to different redistribution protocols which result in different reactant distributions can be found, e.g. in [10,16,17]. In the present study the focus lies on the coupling of the population balance with a complex flow structure. Therefore, only the limiting case of equal repulsive and cooperative forces is being investigated.

For this limiting case P_{2D}^{eq} is calculated from two one-dimensional Poisson distributions P_A and P_B of both reactants by

$$P_{2D}^{eq}(i,\, j,\, t) = P_A(i,\, t) \cdot P_B(j,\, t) \quad \text{with} \quad i,\, j = 0 \ldots N_{l,max}. \tag{5}$$

The two one-dimensional Poisson distributions are calculated by

$$P_A(i,\, t) = \lambda_A(t)^i \, e^{-\lambda_A(t)/i!} \quad \text{with} \quad \lambda_A(t) = \frac{N_A^{total}(t)}{N_M(t)} \tag{6}$$

and

$$P_B(j,\, t) = \lambda_B(t)^j \, e^{-\lambda_B(t)/j!} \quad \text{with} \quad \lambda_B(t) = \frac{N_B^{total}(t)}{N_M(t)}. \tag{7}$$

Thus, only λ_A and λ_B have to be known for the determination of P_{2D}^{eq}. Both represent the mean occupancies of a droplet with barium and sulfate ions, which are defined by the ratios of the total number of A or B ions and the total number of droplets in the reactor. The total numbers of A and B ions are given by

$$N_A^{total}(t) = (N_M(t) - N_{M,0}) \cdot \lambda_{A,0,feed} - N_s(t) \tag{8}$$

$$N_B^{total}(t) = N_{M,0} \cdot \lambda_{B,0} - N_s(t) \tag{9}$$

and the total number of droplets $N_M(t)$ is calculated by Eq. (12). $N_{M,0}$ is the initial number of droplets, $\lambda_{A,0,feed}$ the initial mean droplet occupancy with A ions in the feed, $\lambda_{B,0}$ the initial droplet occupancy with B ions inside the reactor and $N_s(t)$ is the total number of $BaSO_4$ molecules in solid state calculated by Eq. (11).

3.1.3. Balance equations

To calculate the two Dirac-delta functions (Eq. (4)) in order to close the reduced population balance model the balance equations for $N_0(t)$, $N_s(t)$ and $N_M(t)$ have to be solved and the time evolution of $\bar{N}_P$ has to be derived from these equations:

$$\frac{dN_0(t)}{dt} = -\sum_{i=N_{crit}}^{N_{l,max}} \sum_{j=N_{crit}}^{N_{l,max}} P_{2D}^{eq}(i,\, j,\, t) \cdot r_{nuc}(i,\, j) \cdot V_W(t) + N_{feed}(t), \tag{10}$$

$$\frac{dN_s(t)}{dt} = \sum_{i=N_{crit}}^{N_{l,max}} \sum_{j=N_{crit}}^{N_{l,max}} M_M(i,\, j) \cdot P_{2D}^{eq}(i,\, j,\, t) \cdot r_{nuc}(i,\, j) \cdot V_W(t) + \sum_{i=1}^{N_{l,max}} \sum_{j=1}^{N_{l,max}} P_{2D}^{eq}(i,\, j,\, t) \cdot r_{gro}(i,\, j) \cdot \Psi_T(t) \cdot (N_M(t) - N_0(t)) \tag{11}$$

and

$$\frac{dN_M(t)}{dt} = N_{feed}(t), \tag{12}$$

where N_{crit} is the critical number of molecules needed to form a stable nucleus (defined by the modified Gibbs–Thomson relation, see Eq. (19)), $N_{l,max}$ the maximum number of dissolved ions of one kind inside a droplet, r_{nuc} the nucleation rate, V_W the water volume, N_{feed} the feed rate of droplets, r_{gro} the growth rate and $\psi_T(t)$ is a transformation factor for the growth rate (see Eq. (14)). The matrix M_M correlates the ion combination $i,\cdot j$ with the number of ions involved in the phase transition to solid state (example: five barium ions and seven sulfate ions can only form a $BaSO_4$ particle consisting of five molecules → $M_M(5,7) = 5 = \min(5,7)$).

The mean number of $BaSO_4$ molecules within one particle needed for the localization of the second Dirac-delta function in Eq. (4) can be determined from all three balances by

$$\bar{N}_P(t) = \frac{N_s(t)}{N_M(t) - N_0(t)}. \tag{13}$$

The factor $\psi_T(t)$ in Eq. (11) transforms the generally used unit for growth rates (m/s) in the unit used in the discrete balances of our model framework ((number of molecules)/s). It is defined as the first derivative of the mean number of molecules within one particle $\bar{N}_P$ with respect to the mean particle diameter:

$$\Psi_T(t) = \frac{d\bar{N}_P(\bar{d}_P(t))}{d\bar{d}_P(t)} = \frac{d}{d\bar{d}_P(t)} \left(\frac{k_V \cdot \rho_P \cdot N_{Avogadro}}{M_P} \cdot \bar{d}_P^3(t) \right) = 3 \cdot \frac{k_V \cdot \rho_P \cdot N_{Avogadro}}{M_P} \cdot \bar{d}_P^2(t) \tag{14}$$

with

$$\bar{d}_P^3 = \frac{M_P}{k_V \cdot \rho_P \cdot N_{Avogadro}} \cdot \bar{N}_P, \tag{15}$$

where M_P is the molar mass of $BaSO_4$, k_V the volume shape factor, ρ_P the particle density and $N_{Avogadro}$ is the Avogadro's number.

3.1.4. Precipitation kinetics

Nucleation and growth rates strongly depend on the supersaturation S within each droplet. For the microemulsion system with discrete coordinates individual supersaturation ratios for each droplet class depending on the ion combination are present. Thus nucleation and growth rates have as well individual values for each droplet class. The supersaturation for each droplet class

is given by

$$S(N_A, N_B) = \sqrt{\frac{c_A(N_A) \cdot c_B(N_B)}{k_L}} = \sqrt{\frac{N_A \cdot N_B}{k_L \cdot N_{Avogadro}^2 \cdot V_D^2}} \quad (16)$$

with V_D being the droplet volume and k_L the solubility product.

Special kinetic approaches for precipitation inside microemulsion droplets cannot be found in the literature. In this study modified approaches from bulk precipitation were used to describe the particle formation dynamics. The nucleation rate is related to the standard approach by Bałdyga et al. [18] with $\alpha_{nuc} = 15$ for high supersaturation. It is given by

$$r_{nuc}(N_A, N_B) = k_{nuc}^{eff} \cdot (S(N_A, N_B) - 1)^{\alpha_{nuc}}. \quad (17)$$

The implemented growth rate:

$$r_{gro}(N_A, N_B) = k_{gro}^{eff} \cdot (S(N_A, N_B) - 1)^{\alpha_{gro}} \quad (18)$$

is a modified standard bulk phase approach by Nielsen [19] with $\alpha_{gro} = 2$. The effective nucleation and growth rate constants k_{nuc}^{eff} and k_{gro}^{eff} are estimated by a least square optimization algorithm. The particle size distributions obtained with the model represented by Eq. (3) and the experimentally obtained particle size distributions are fitted simultaneously for 11 different experiments (details about the parameter estimation can be found in [10,13]).

Another important parameter for the nucleation kinetics is the critical number of molecules needed to form a stable nucleus N_{crit}. The Gibbs–Thomson relation:

$$N_{crit}(N_A, N_B) = \frac{32 \cdot \pi \cdot M_P^2}{\rho_P^2 \cdot N_{Avogadro}^2} \cdot \frac{\sigma_{eff}^3}{3} \cdot \times (k_B \cdot T \ln(S(N_A, N_B)))^{-3} \quad (19)$$

is used to calculate N_{crit}. This value depends on the supersaturation as well and is therefore also droplet-class specific. In Eq. (19) σ_{eff} is the effective interfacial surface tension, k_B the Boltzmann constant and T is the temperature. Niemann and Sundmacher [13] showed that σ_{eff} is approximately 0.13 J/m^2 in the investigated system. Consequently, the resulting N_{crit} values are between 8 and 9 according to the droplet class.

Table 3
Model parameters

Maximum number of dissolved ions per droplet, $N_{l,max}$	30
Droplet feed rate, N_{feed} ($\times 10^{17}$ s^{-1})	2.4
Initial number of droplets inside the reactor, $N_{M,0}$ ($\times 10^{19}$)	6.3
Molar mass of barium sulfate, M_P (g/mol)	233.39
Density of barium sulfate, ρ_P (g/cm^3)	4.48
Volume shape factor, k_V	$\pi/6$
Solubility product, k_L ($\times 10^{-10}$ mol^2/l^2)	1.3
Effective nucleation rate constant, k_{nuc}^{eff} ($\times 10^{41}$ (m^3 s)$^{-1}$)	5.2
Effective growth rate constant, k_{gro}^{eff} (nm/s)	145.1

Table 3 contains all parameters used in the simulations.

3.2. Numerical computations

The simplified PBM explained above has been first applied for the homogeneous reaction process (zero-dimensional analysis) before performing the inhomogeneous computations (three-dimensional analysis in space).

3.2.1. Zero-dimensional analysis

The homogeneous case calculations as a function of only time have been performed by MATLAB® 7.0. The computation at this stage takes less than a second when employing a single Pentium-IV Linux PC (2.7 GHz/2 GB memory). The results obtained from these time-dependent calculations are discussed later when compared with those obtained by experiments and coupled CFD simulations.

3.2.2. Three-dimensional CFD simulations

The geometry and the unstructured grid of the reactor used in the experiments have been generated using MixSim® 2.0 and are shown in Fig. 2. There are about 80,000 volume elements in the whole domain. This grid resolution has been obtained following the best practice guidelines proposed by MixSim® and FLUENT® [20,21]. Although the operation is in semi-batch mode (which means increasing fluid volume) until the end of feeding, the influence of the volume change on the flow field has not been modelled in order to sim-

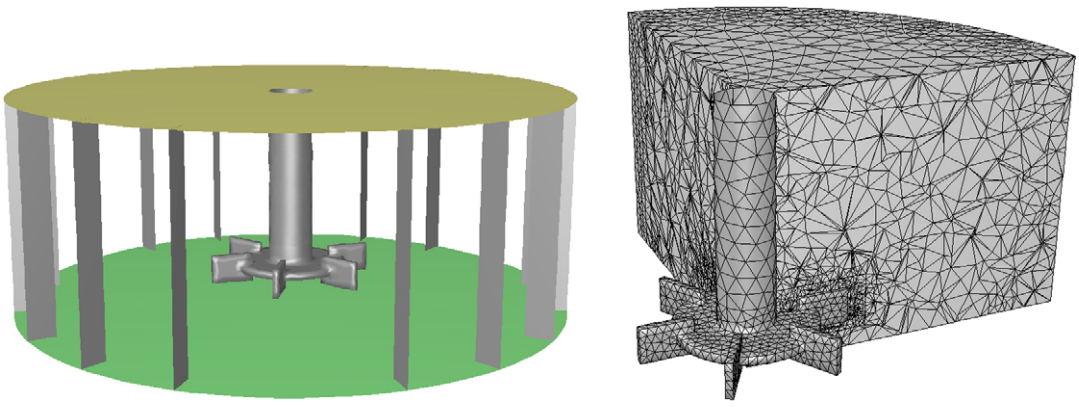

Fig. 2. Geometry (left) and computational grid of the reactor (right) (complete dimensions are given in [2,3]).

plify the computations. Instead, the total volume of the two microemulsions has been taken into account assuming a batch system during the whole simulation. Otherwise, applying a deforming dynamic mesh model for the changing liquid level would increase drastically the complexity and the computing time of the calculations. This is due to the fact that the flow parameters should be extrapolated to the deformed and newly created volume elements, associated with the requirement to re-compute the full flow field after each time step. Nevertheless, the injection process is fully taken into account in the simulation during the feed time of 257.14 s. The feeding point is identical with the experiments and can be seen in Fig. 7.

The three-dimensional, unsteady simulations have been performed with the industrial CFD code FLUENT® 6.2. Equations and source terms of the reaction kinetics and PBM have been defined via external user-defined scalars (UDS) and functions (UDF). A two-stage calculation has been implemented. First, the flow field has been simulated without the reaction process until the unsteady hydrodynamic conditions have reached a constant limit cycle for one impeller rotation. Afterwards, the reaction process has been simulated within Fluent by switching off the flow and the turbulence models (i.e. using the frozen-flow conditions corresponding to the limit cycle), while activating chemical reactions. By this way, the computations can be considerably accelerated. The computing times are about 24 h for the first stage and 6 up to 32 h for the second stage (depending on the simulated process duration), employing the same standard PC mentioned previously. This two-stage calculation method has already been applied for other processes (for example for crystallization reactors [22,23]) and found to be accurate (good agreement with experimental data) and computationally very efficient (low computing time). As an alternative, performing directly the calculation in a fully coupled manner (i.e. simultaneously solving for flow, turbulence and chemical reactions in time) results in a drastically higher computational effort. For example, to compute 30 s in real time for the process, the simulation relying on frozen flow conditions (two-stage calculation) takes about 21 min, while the corresponding fully coupled simulation (single-stage calculation) requires slightly less than 60 days. Both calculations lead to almost identical results in the present configuration [4].

Two numerical approaches have been employed in order to simulate the motion of the impeller. The so-called multiple reference frames (MRF) model has initially been applied, yielding a first estimation of the flow for steady-state conditions. The obtained MRF-solution has been used as an initial guess for a further, unsteady simulation applying the more realistic sliding mesh model (SMM). Unlike the MRF model [24], the SMM is capable of taking into account the impeller-baffle coupling effects, since the time-dependent location of the impeller is taken into consideration [25–28]. Therefore the sliding mesh technique delivers more reliable results for an unsteady calculation. However, initializing the SMM-simulation using the MRF-results reduces the total computational time considerably [29], compared to a direct SMM-simulation. The computing times for the MRF- and SMM-simulations are roughly 3 h and 21 h, respectively, until the cyclic unsteady flow field (i.e. the right flow periodicity) has been obtained. For these flow field simulations a second order discretization has been used in space and a second order implicit time formulation has been chosen for the unsteady solution of the SMM [21]. Iterations have been stopped when residuals fall below 10^{-4} for continuity and below 10^{-3} for the other parameters in each time step.

The standard k–ε approach has been used as turbulence model since this model is known to supply a reasonable accuracy and short computing times for such baffled tanks in which no strong, swirling flow occurs [30,31].

4. Results and discussion

4.1. Validation of the reduced model

The reduced PBM has been validated using the available experimental results. Fig. 3 shows the comparison for particle size distributions obtained by numerical and experimental results for the different conditions (see Table 1). Here it is worth keeping in mind that the reduced model yields only the mean particle size instead of a complete distribution function. As can be seen from these comparisons an acceptable agreement has been achieved with the reduced model, although larger deviations are observed for cases with a high concentration excess of one of the microemulsions. This validation procedure, carried out for spatially homogeneous conditions (zero-dimensional computation in physical space) forms the basis of the further three-dimensional, inhomogeneous CFD computations.

4.2. Results of CFD simulations

Time-periodic flow conditions have been achieved after roughly 100 full rotations of the impeller (corresponding to 20 s physical time) during the unsteady flow field simulation employing SMM.

The evolution of the mean number of dissolved Ba^{2+} and $SO_4{}^{2-}$ ions per droplet (λ_{Ba}, i.e. λ_A and λ_{SO_4}, i.e. λ_B, respectively) and the mean particle diameter ($\bar{d}_P$) with respect to time according to the three-dimensional (3D) second-stage simulations (including only the inhomogeneous precipitation on top of the frozen flow) are represented in Figs. 4–6 in comparison with the results of the zero-dimensional (0D) analysis in space. Here it is worth stating that each 3D result is an overall mass-averaged value in the whole reactor. Referring to these comparisons, it can be concluded that an almost homogeneous reaction process is observed in the reactor except for Case A, where a noticeable discrepancy is observed compared to the 0D results (relative reduction of the mean, final particle size by 14.1%). This is actually not unexpected since Case A leads to the highest supersaturation ratio in this work. Higher supersaturation ratio leads to a faster reaction, which means greater sensitivity of the process to local hydrodynamic conditions. In other words, the mixing mechanism becomes more impor-

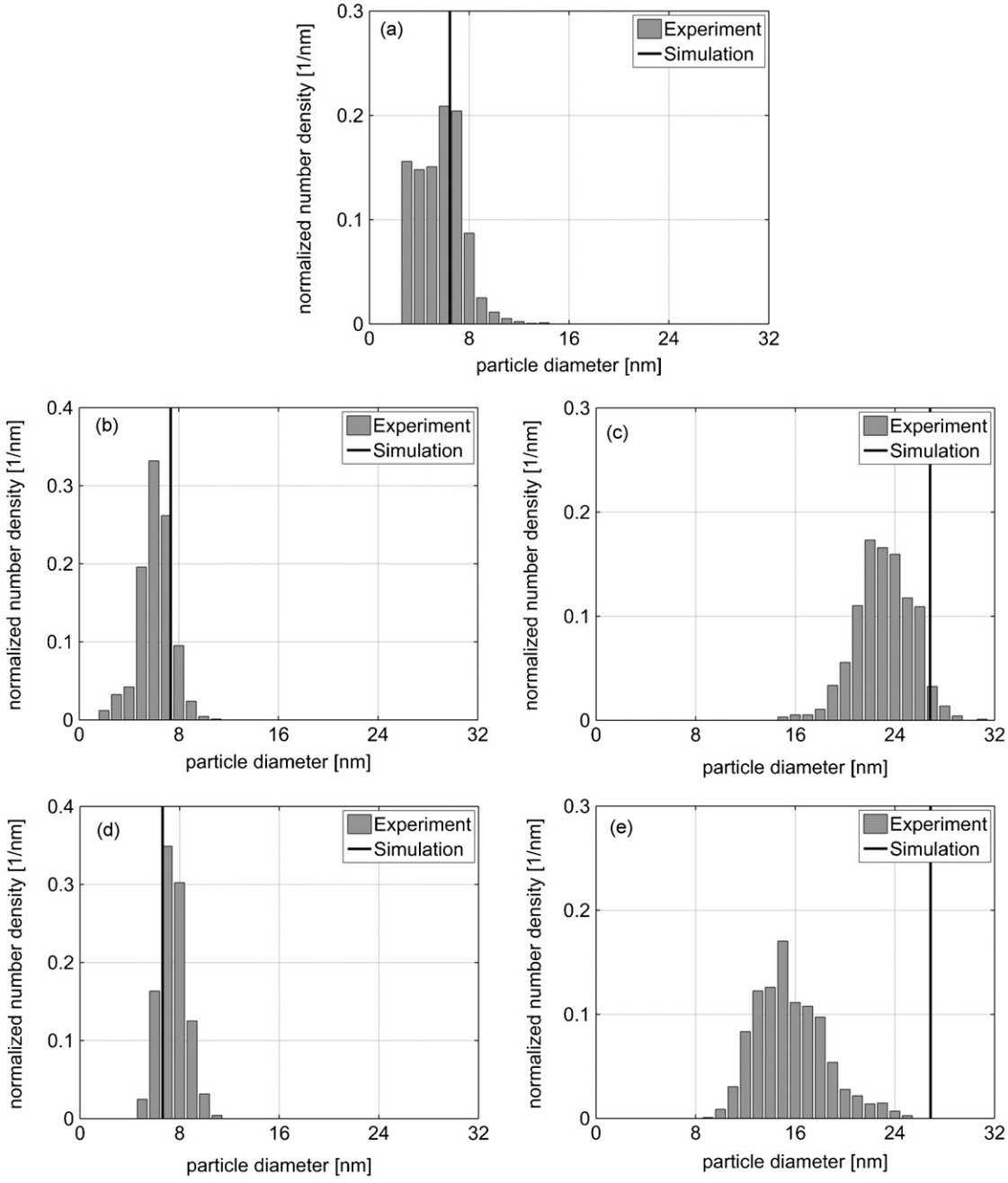

Fig. 3. Validation of the reduced model with experimental data for Cases A (a), B1 (b), B2 (c), C1 (d) and C2 (e).

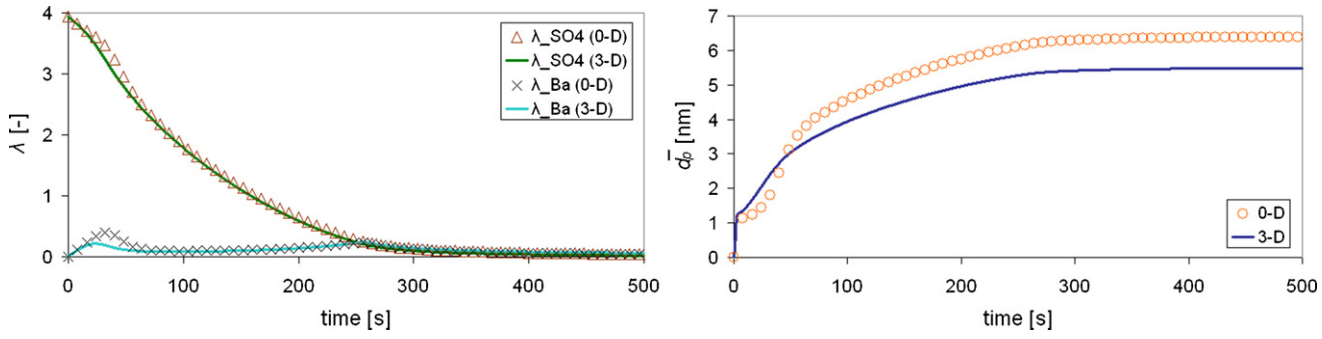

Fig. 4. 0D and 3D calculation results of Case A in comparison.

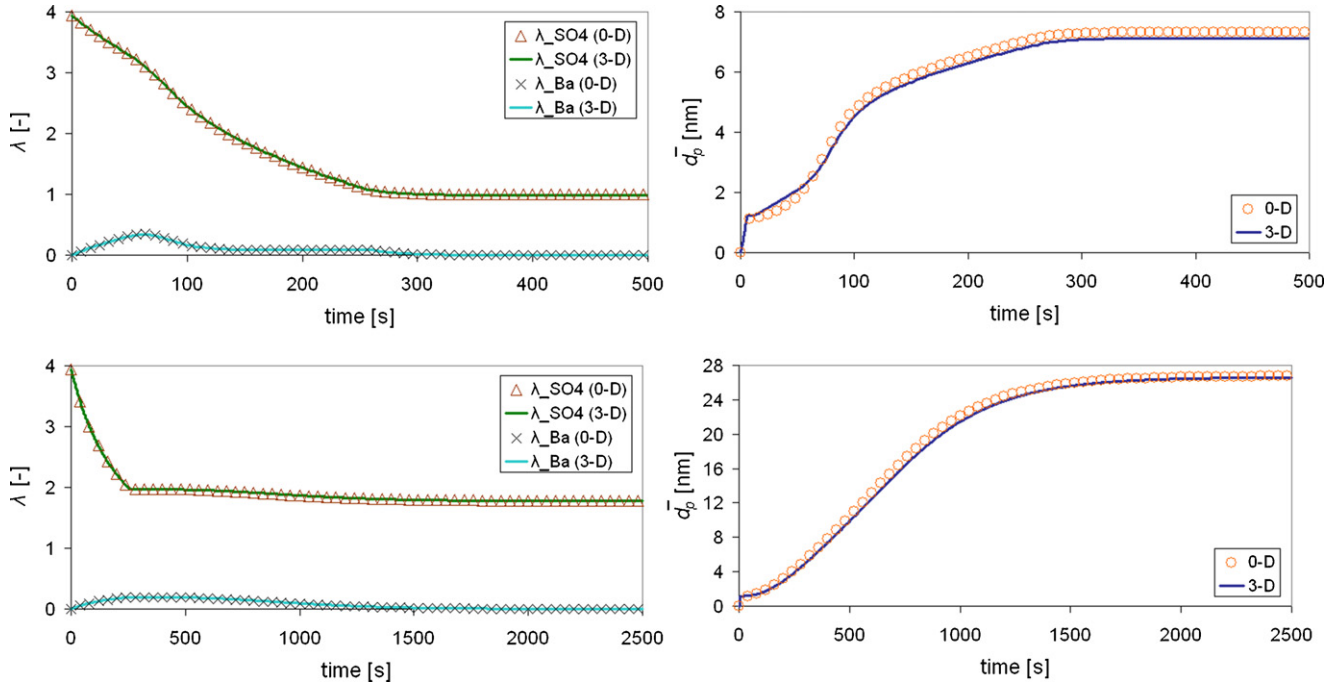

Fig. 5. 0D and 3D calculation results of Cases B1 (top) and B2 (bottom) in comparison.

tant for the precipitation process, since the reaction time scale decreases with increasing supersaturation ratio while the mixing time scale remains unchanged. This situation can be better understood when reaction and macromixing (i.e. reactor-scale mixing) time scales are compared. The reaction time scale, τ_R, for Case A is about 400 s whereas it is around 2000 s for Cases B2 and C2 (see again Figs. 4–6). On the other hand, the mixing time scale, τ_M, is the same for all cases and can be calculated by the following formula for Rushton turbine impellers [18]:

$$\tau_M = \frac{V_{reactor}}{Q_c} \tag{20}$$

with

$$Q_c = 1.5 N_{rps} d_{imp}^3, \tag{21}$$

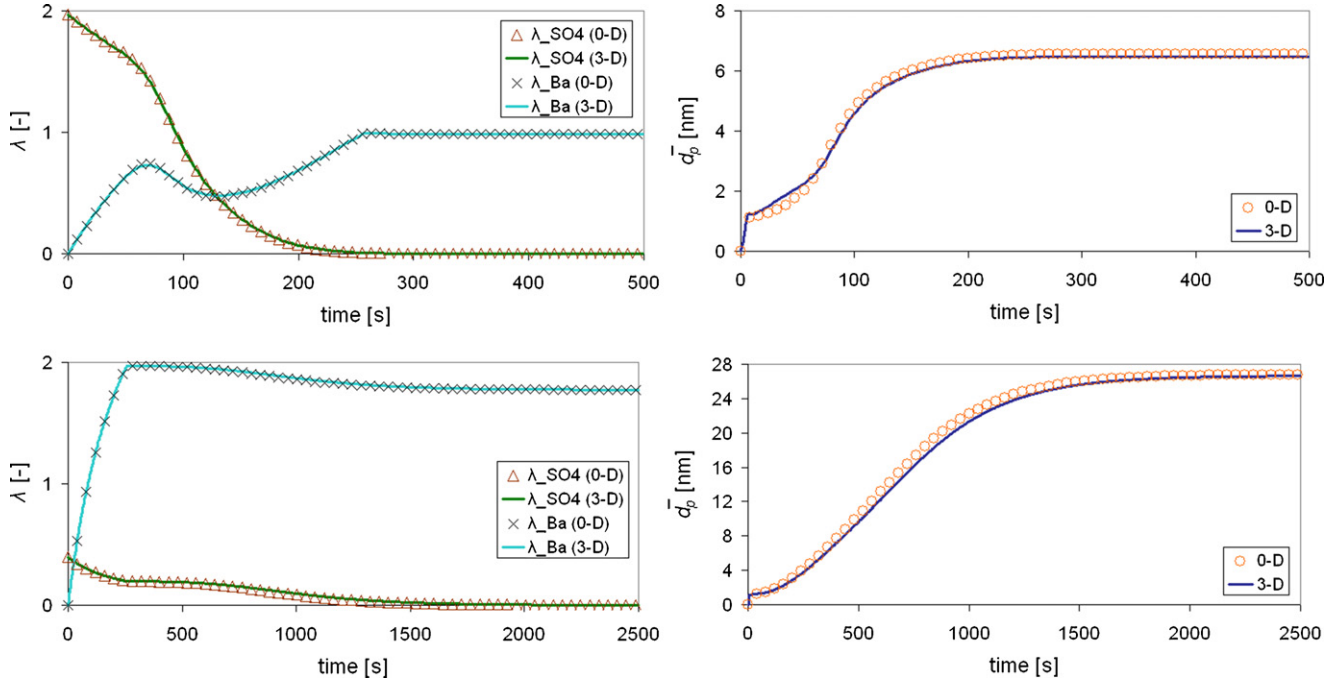

Fig. 6. 0D and 3D calculation results of Cases C1 (top) and C2 (bottom) in comparison.

where Q_c is the circulation capacity, N_{rps} the stirring rate and d_{imp} is the impeller diameter, here equal to 3 cm. According to Eqs. (20) and (21), the value of τ_M varies between 0.74 and 1.48 s since the reactor volume, $V_{reactor}$, continuously increases until the end of feeding. As a consequence, $\tau_R \gg \tau_M$ in all cases (well-mixed conditions), but the case with the lowest τ_R value (Case A) is roughly five times more sensitive to mixing conditions compared to Cases B2 and C2. Consequently, almost no deviation between the results of 0D and 3D simulations is observed in Cases B2 and C2 due to the corresponding, low supersaturation levels (the lowest in this study) and therefore long reaction time scales. Finally, Cases B1 and C1 are associated with a visible but very low difference between 0D and 3D simulations.

In addition to these averaged profiles, various local profiles inside the reactor have also been investigated for a better understanding of the mixing conditions. This has been carried out by examining the profiles at six chosen locations, shown in Fig. 7. As can be seen from this sketch, the odd numbered points and the even numbered points are positioned symmetrically to each other with respect to the reactor axis. P3 represents the feed exit location whereas P1 and P5 are placed close to the impeller blades and to the fluid top level, respectively. The local λ_{Ba}, λ_{SO_4}, and $\bar{d}_P$ profiles are examined at these locations for two extreme cases: Case A (for which the effect of hydrodynamic conditions are maximum because of the highest supersaturation ratio) and Case B2 (for which the mixing should have a minimum influence on the reaction due to the lowest supersaturation level). Corresponding time-dependent results are given in Figs. 8 and 9. According to these figures, higher local deviations from the reactor mean are observed in Case A, as expected. The largest local discrepancies in both cases belong obviously to the feeding exit point (P3), due to the continuously injected fresh reactant that causes a locally varying supersaturation profile. Moreover, the P5 profiles show also a non-negligible deviation in Case A, which is due to a flow recirculation vortex transporting the fed

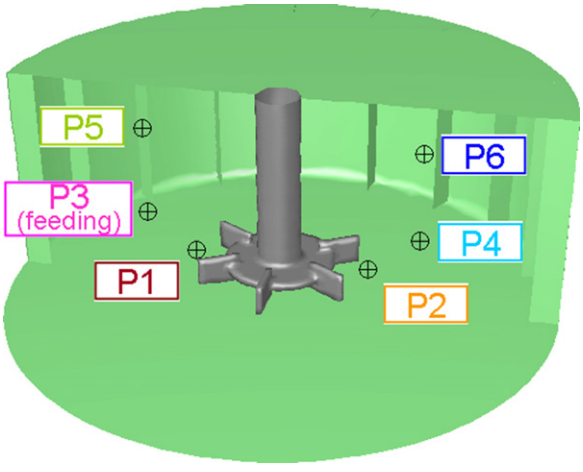

Fig. 7. Positions of the six points at which the local profiles are observed (note that the colours are identical with those used for the profiles).

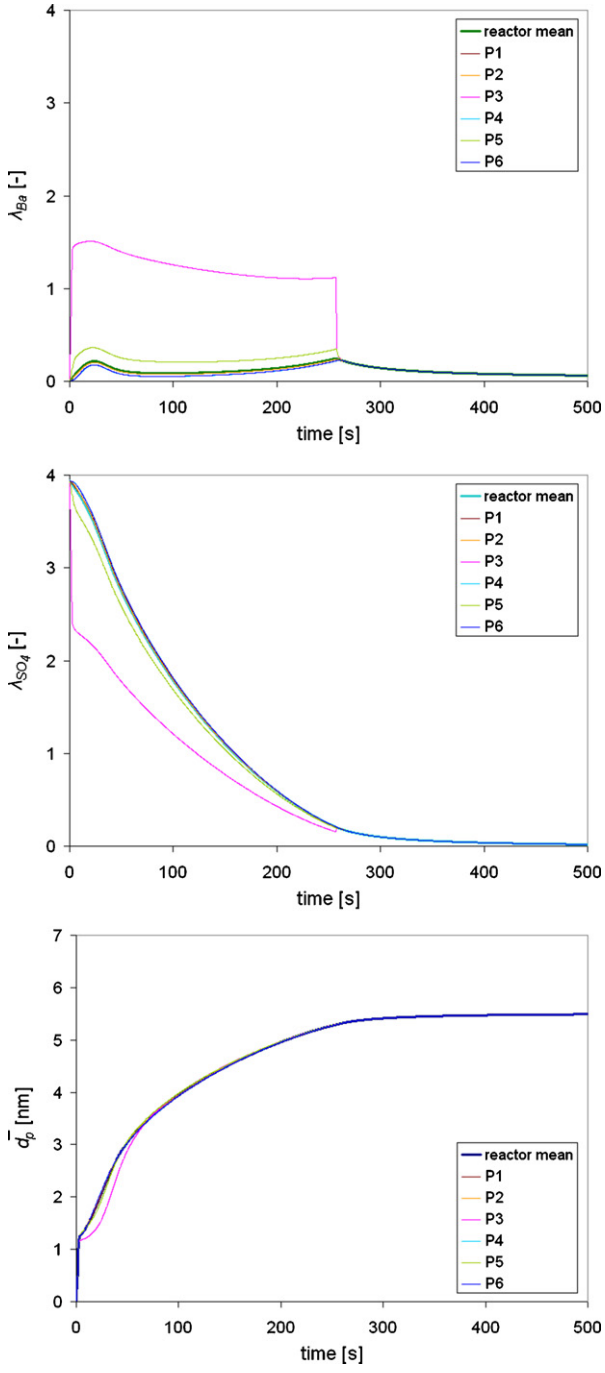

Fig. 8. Local profiles in comparison with reactor mean (thick line) for Case A. Feeding is completed at time $t = 257.14$ s.

droplets of concentrated reactant from the feed point directly to this region within a short time. However, all local discrepancies disappear very rapidly after the feeding is completed ($t = 257.14$ s). This confirms that the mixing conditions induced by the impeller are strong enough to homogenize the emulsion system in a very short time. All locations other than P3 and P5 are always almost identical to the mean conditions within the reactor.

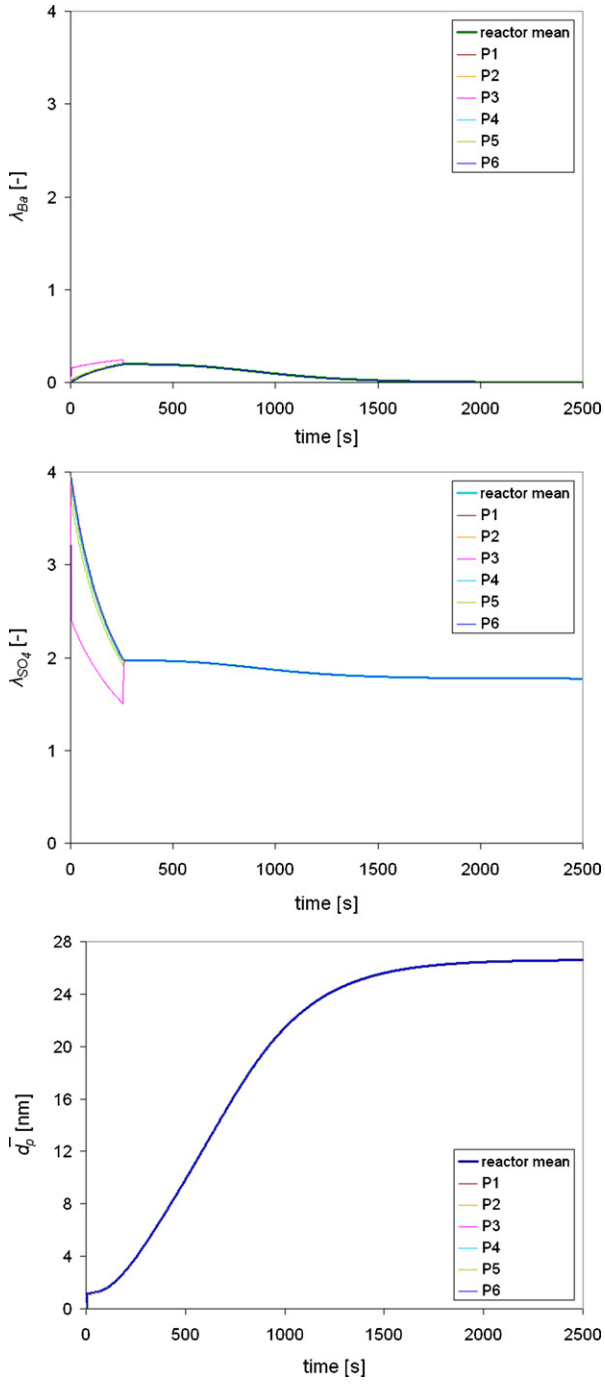

Fig. 9. Local profiles in comparison with reactor mean (thick line) for Case B2. Feeding is completed at time $t = 257.14$ s.

5. Conclusion

The aim of this work was to develop a simplified, zero-dimensional (homogeneous) PBM describing the precipitation of $BaSO_4$ in a microemulsion droplet population and to implement this model for the three-dimensional, real case analysis of the reaction process in a semi-batch reactor. The PBM is based on a two-dimensional Poisson distribution for the dissolved Ba^{2+} and $SO_4{}^{2-}$ ions and on a simplified representation of the droplet number distribution by two Dirac-delta functions.

Although the obtained results of zero-dimensional computations for stoichiometric cases have shown a good agreement with the experimental data, bigger deviations have been observed for cases with a high concentration excess of one of the microemulsions. Nevertheless, the reduced model has been validated up to an acceptable degree with the help of experimental data via this initial analysis.

In the second step, inhomogeneous simulations in space have been performed for a more realistic investigation by embedding the reduced PBM formulation within an industrial CFD code. The results of these three-dimensional CFD computations show an almost homogeneous reaction process within the reactor, which leads to the conclusion that the mixing quality is high. Noticeable discrepancies compared to zero-dimensional computations have been observed only in the stoichiometric case, for which the supersaturation ratio is highest. Furthermore, local deviations from the reactor mean can only be identified in the vicinity of the feeding location. This means that the deviations obtained with the simplified PBM model far from stoichiometry do not result from a coupling with hydrodynamics.

Nevertheless, the resulting coupled PBM/CFD simulation tool is extremely useful. Acceptable computing times have been obtained by using the flow field results based on a MRF approach as an initial guess for the more accurate calculations employing SMM. Furthermore, the reaction is solved as a final step on top of the frozen, cyclic flow condition. By this way, it is possible to investigate the reaction process for any kind of three-dimensional inhomogeneous hydrodynamic conditions. This situation offers excellent opportunities for reactor optimization as a further step, by trying to use hydrodynamics in a controlled manner in order to improve process quality, for example to obtain smaller particles.

References

[1] W. Luther, Industrial Application of Nanomaterials—Chances and Risks. Technological Analysis, Future Technologies Division of VDI Technologiezentrum GmbH, Düsseldorf, Germany, 2004.
[2] B. Niemann, F. Rauscher, D. Adityawarman, A. Voigt, K. Sundmacher, Microemulsion-assisted precipitation of particles: experimental and model-based process analysis, Chem. Eng. Proc. 45 (2006) 917–935.
[3] D. Adityawarman, A. Voigt, P. Veit, K. Sundmacher, Precipitation of $BaSO_4$ nanoparticles in a non-ionic microemulsion: identification of suitable control parameters, Chem. Eng. Sci. 60 (2005) 3373–3381.
[4] A.A. Öncül, B. Niemann, D. Thévenin, K. Sundmacher, CFD model of a semi-batch reactor for the precipitation of nanoparticles in the droplets of a microemulsion, in: Proceedings of 16th European Symposium on Computer Aided Process Eng. (ESCAPE16) & 9th International Symposium on Process Systems Eng. (PSE2006), Garmisch-Partenkirchen, Germany, 2006, ISBN 978-0-444-52257-3, pp. 203–208.
[5] K.W. Min, W.H. Ray, The computer simulation of batch emulsion polymerization reactors through a detailed mathematical model, J. Appl. Polym. Sci. 22 (1978) 89–112.
[6] E. Unzueta, J. Forcada, Modeling the effect of mixed emulsifier systems in emulsion copolymerization, J. Appl. Polym. Sci. 66 (1997) 445–458.
[7] C. Kiparissides, Challenges in particulate polymerization modeling and optimization: a population balance perspective, J. Process Control 16 (2006) 205–224.
[8] H.M. Vale, T.F. McKenna, Modeling particle size distribution in emulsion polymerization reactors, Prog. Polym. Sci. 30 (2005) 1019–1048.

[9] R. Singh, S. Kumar, Effect of mixing on nanoparticle formation in micellar route, Chem. Eng. Sci. 61 (2006) 192–204.
[10] B. Niemann, K. Sundmacher, Emulsionsgestützte Synthese von Nanopartikeln: Experimentelle und modelltheoretische Prozessanalyse, DECHEMA/GVC Jahrestagungen, Wiesbaden, Germany, 2006.
[11] B. Niemann, K. Sundmacher, Manipulation and control of the particle size distribution of nanoparticles during their formation in microemulsion droplets by a suitable feed strategy, in: Proceedings of AIChE Annual Meeting, San Francisco, USA, 2006, ISBN 0-8169-1012-X, Paper No: 87e.
[12] B. Niemann, K. Sundmacher, Nanoparticle precipitation in microemulsion: a discrete-continuous population balance approach, in: Proceedings of PARTEC 2007, Nuremberg, Germany, 2007.
[13] B. Niemann, K. Sundmacher, A discrete-continuous population balance approach for the nanoparticle precipitation in microemulsions, in: World Congress on Particle Technology, vol. 5, Orlando, USA, 2006.
[14] S.S. Atik, J.K. Thomas, Transport of photoproduced ions in water in oil microemulsions—movement of ions from one water pool to another, J. Am. Chem. Soc. 103 (1981) 3543–3550.
[15] T.A. Hatton, A.S. Bommarius, J.F. Holzwarth, Population-dynamics of small systems. 1. Instantaneous and irreversible reactions in reversed micelles, Langmuir 9 (1993) 1241–1253.
[16] R. Jain, A. Mehra, Monte Carlo models for nanoparticle formation in two microemulsion systems, Langmuir 20 (2004) 6507–6513.
[17] U. Natarajan, K. Handique, A. Mehra, J.R. Bellare, K.C. Khilar, Ultrafine metal particle formation in reverse micellar systems: effects of intermicellar exchange on the formation of particles, Langmuir 12 (1996) 2670–2678.
[18] J. Bałdyga, W. Podgórska, R. Pohorecki, Mixing precipitation model with application to double feed semibatch precipitation, Chem. Eng. Sci. 50 (1995) 1281–1300.
[19] A.E. Nielsen, Electrolyte crystal-growth mechanisms, J. Cryst. Growth 67 (1984) 289–310.
[20] MixSim 2.0 User's Guide, Fluent Inc., Lebanon, USA, 2003.
[21] Fluent 6.2 User's Guide, Fluent Inc., Lebanon, USA, 2005.
[22] A.A. Öncül, D. Thévenin, M.P. Elsner, A. Seidel-Morgenstern, Numerical analysis of the preferential crystallization of enantiomers, in: Proceedings of 11th Workshop on Two-phase Flow Predictions, Halle, Germany, 2005, ISBN 3-86010-767-4, pp. 5.10/1–5.10/15.
[23] A.A. Öncül, D. Thévenin, M.P. Elsner, A. Seidel-Morgenstern, Numerical analysis of the preferential crystallization of enantiomers in complex flows, in: Proceedings of 12th International Workshop on Industrial Crystallization (BIWIC12), Halle, Germany, 2005, ISBN 3-86010-797-6, pp. 165–172.
[24] J.Y. Luo, R.I. Issa, A.D. Gosman, Prediction of impeller-induced flows in mixing vessels using multiple frames of reference, IChemE Symp. Ser. 136 (1994) 549–556.
[25] J.Y. Luo, A.D. Gosman, R.I. Issa, J.C. Middleton, M.K. Fitzgerald, Full flow field computation of mixing in baffled stirred vessels, Chem. Eng. Res. Des. 71A (1993) 342–344.
[26] K. Ng, N.J. Fentiman, K.C. Lee, M. Yianneskis, Assessment of sliding mesh CFD predictions and LDA measurements of the flow in a tank stirred by a Rushton impeller, Chem. Eng. Res. Des. 76A (1998) 737–747.
[27] G. Montante, K.C. Lee, A. Brucato, M. Yianneskis, Numerical simulations of the dependency of flow pattern on impeller clearance in stirred vessels, Chem. Eng. Sci. 56 (2001) 3751–3770.
[28] M. Sommerfeld, S. Decker, State of the art and future trends in CFD simulation of stirred vessel hydrodynamics, Chem. Eng. Technol. 27 (2004) 215–224.
[29] E.L. Paul, V.A. Atiemo-Obeng, S.M. Kresta, Handbook of Industrial Mixing: Science and Practice, Wiley-Interscience, Hoboken, NJ, USA, 2004.
[30] G. Montante, K.C. Lee, A. Brucato, M. Yianneskis, Experiments and predictions of the transition of the flow pattern with impeller clearance in stirred tanks, Comput. Chem. Eng. 25 (2001) 729–735.
[31] G. Montante, A. Bakker, Stirring up the phases in tall tanks, Fluent News XIII (2) (2004) 8–9.